

Accepted Manuscript

Coupling of the electrochemical oxidation (EO-BDD)/photocatalysis (TiO₂-Fe-N) processes for degradation of acid blue BR dye

Ulises Morales, Carlos J. Escudero, María J. Rivero, Inmaculada Ortiz, Juan Manríquez Rocha, Juan M. Peralta-Hernández



PII: S1572-6657(17)30894-9
DOI: doi:[10.1016/j.jelechem.2017.12.014](https://doi.org/10.1016/j.jelechem.2017.12.014)
Reference: JEAC 3719
To appear in: *Journal of Electroanalytical Chemistry*
Received date: 27 September 2017
Revised date: 30 November 2017
Accepted date: 8 December 2017

Please cite this article as: Ulises Morales, Carlos J. Escudero, María J. Rivero, Inmaculada Ortiz, Juan Manríquez Rocha, Juan M. Peralta-Hernández, Coupling of the electrochemical oxidation (EO-BDD)/photocatalysis (TiO₂-Fe-N) processes for degradation of acid blue BR dye. The address for the corresponding author was captured as affiliation for all authors. Please check if appropriate. Jeac(2017), doi:[10.1016/j.jelechem.2017.12.014](https://doi.org/10.1016/j.jelechem.2017.12.014)

This is a PDF file of an unedited manuscript that has been accepted for publication. As a service to our customers we are providing this early version of the manuscript. The manuscript will undergo copyediting, typesetting, and review of the resulting proof before it is published in its final form. Please note that during the production process errors may be discovered which could affect the content, and all legal disclaimers that apply to the journal pertain.

**Coupling of the electrochemical oxidation (EO-BDD)/photocatalysis
(TiO₂-Fe-N) processes for degradation of acid blue BR dye**

Ulises Morales¹, Carlos J. Escudero², María J. Rivero², Inmaculada Ortiz²,
Juan Manríquez Rocha³, Juan M. Peralta-Hernández^{1*}

¹*Departamento de Química, División de Ciencias Naturales y Exactas, Campus
Guanajuato. Universidad de Guanajuato, Guanajuato, Gto. 36050, Mexico.*

²*Department of Chemical and Biomolecular Engineering, ETSIT, University of Cantabria,
Avda. de los Castros, s/n, 39005 Santander, Spain.*

³*CIDETEQ, S. C., P.O. Box 064, C.P. 76703, Parque Tecnológico Querétaro S/N,
Sanfandila, Pedro Escobedo, Querétaro, Mexico.*

*Corresponding author: juan.peralta@ugto.mx

www.ugto.mx

Abstract

We report on the successful preparation of Fe-N codoped Titania powders, using TiO₂ Degussa P25, salt of Fe (II), and Urea. Modified Titania-based materials were characterized by SEM, EDS, BET, Raman, XRD diffraction and diffuse reflectance UV-vis spectroscopy measurements. The doping of TiO₂ induced a shift in the absorption threshold towards the spectral range, obtaining catalysts with a greater photoactivity than the one of pure Degussa P25. The degradation of 200 mL of a solution with 50 mgL⁻¹ acid blue BR dye in sulfate medium at pH 3.0 has been comparatively studied by electrochemical oxidation using a boron doped diamond anode (EO-BDD), Photocatalysis TiO₂-Fe-N, and coupled material of EO-BDD/Photocatalysis TiO₂-Fe-N. The solution was slowly degraded by EO-BDD (25%) and single Photocatalysis TiO₂-Fe-N because of the low rate of dye degradation and its colored by-products with hydroxyl radicals generated at the BDD anode and catalyst surface from water oxidation (29%), whereas the solution was more rapidly degraded using coupled material of EO-BDD/Photocatalysis TiO₂-Fe-N (82%), owing to the additional generation of hydroxyl radicals from the photocatalysis of TiO₂-Fe-N and BDD anode.

Key words: wastewater treatment, Fe-N codoped TiO₂, photoelectrocatalysis, synergistic effect.

1. Introduction

The photocatalysis based on semiconductor has been extensively studied and has become one of the most important methods in environmental protection procedures, such as air and water purification, hazardous waste remediation, and so on [1]. In recent years, a considerable effort has been devoted to the study of metal and nonmetal doped titanium dioxide, in order to improve the photocatalytic efficiency of TiO_2 , in the enhancement of the photoresponse of TiO_2 from ultraviolet to the visible range without decreasing photocatalytic activity [2]. The dopants create changes in the band gap of TiO_2 , which can shift the absorption edge of TiO_2 . Some experimental results have also shown that the incorporation of metal ions in TiO_2 crystal structure can do both: the narrow band gap of TiO_2 reduces the electron-hole recombination rate, and thereby increases the photocatalytic efficiency of TiO_2 using UV light [3]. A systematic study has been conducted of the doping of TiO_2 with 21 metal ions. Fe^{3+} was considered to be a successful doping element due to its half-filled electronic configuration [4]. Nitrogen doping has received much attention due to its low cost and demonstration of the band gap narrowing, with significant improvement in visible light absorption capability [2,5]. Further, nitrogen can be easily introduced in the TiO_2 structure, due to its comparable atomic size with oxygen, small ionization energy, metastable center formation, and stability [6]. Research results showed that the modification of titania by codoping may be a more effective method to improve the photocatalytic activity under UV and visible light [2,7].

In the field of TiO_2 photocatalyzed reactions, electrochemical advanced oxidation processes (EAOPs) have recently received increasing attention for removal of organic contaminants

from wastewater [8,9,10]. Within the EAOPs, the most used process is the electrochemical oxidation (EO), which can be easily applied to electrochemical dyes decolorization. EO consists in the oxidation of pollutants in an electrochemical cell by (1) direct anodic oxidation (i.e., direct electron transfer to the anode), which yields very poor decontamination; (2) indirect or mediated oxidation via chemical reaction with electrogenerated species from water discharge at the anode surface, such as physically adsorbed “active oxygen” or chemisorbed active oxygen [8,9]. Moreover, the EO is a technology that offers additional advantages, such as environmental compatibility, versatility and amenability to automation [11]. The main environmental advantage consists in the compatibility due to the in-situ generation of free hydroxyl radical ($\bullet\text{OH}$) by means of water discharge at the anode surface, essentially without addition of any other chemical reagents [12,13].

To carry out this reaction, at this time, boron doped diamond (BDD) electrodes are considered to be the best anodic materials for EO because they are capable to mineralize a large number of aromatics and aliphatic carboxylic acids [11,14,15,16]. The generation of the physisorbed oxidant $\text{BDD}(\bullet\text{OH})$ proceeds as follows:



In order to obtain a better understanding of the viability of EAOP coupled with the photocatalytic process, a study was carried out to decolorize and degrade a complex dye, an acid blue dye BR which is daily used in the tanning industry in the region of León, Mexico.

This paper presents the results obtained from the comparative decolorization and degradation of blue dye BR solutions in Na_2SO_4 by EO-BDD, Photocatalysis $\text{TiO}_2\text{-Fe-N}$,

and coupled material of EO-BDD/Photocatalysis TiO_2 -Fe-N. The effect of the current applied on their degradation were examined to better clarify the role of each process. The dye degradation were followed by UV-vis determinations and High-resolution liquid chromatography (HPLC).

2. Materials and Methods

The following commercial reagents were used: Titania Degussa P25, iron chloride (II) tetrahydrate (>99% sigma-aldrich), urea (>98% sigma-aldrich), isopropyl alcohol (>99% sigma-aldrich), distilled water (J.T. Baker). All the chemicals were used as any purchased purification. The preparation of Fe-N codoped material TiO_2 was carried out by sol-gel method as follows. First, 1.44 g of TiO_2 was dispersed in 200 mL of isopropyl alcohol under stirring for 120 min, followed by the dropped iron (II) chloride tetra hydrate solution 0.5% wt, and 3 mL urea aqueous solution (25%). Mixture was continuously stirred at room temperature for 24h, finally it was dried at 80 $^{\circ}\text{C}$. The resulting product was calcined in static air at 500 $^{\circ}\text{C}$ for 4 h annealing.

2.1. Characterization

Nitrogen adsorption-desorption isotherms were collected at Micromeritics Tri Star IIPLUS equipment (BET, for specific surface area and porosity evaluation). The sample was degassed at 200 $^{\circ}\text{C}$ for 2 h prior to the measurement. The surface morphologies of the nanoparticles were seen by field emission Scanning Electron Microscopy (FE-SEM, ZEISS, voltage 20 KV). Energy-dispersive X-ray analysis (EDX, voltage 20 KV) was also used for the chemical analysis of the nanoparticles. The Raman spectra were recorded on Thermo-Scientific DXR Raman microscope equipped with a 14 mW laser emitting at 780 ± 0.2 nm. All the spectra were obtained at room temperature using 100% of the laser

power, a slit aperture of 50 μm and 200 scans/spectrum [17]. The XRD diffraction patterns of the samples were measured in a θ - θ Bruker D-8 Advance diffractometer with $\text{CuK}\alpha$ radiation, a graphite secondary-beam monochromator, and a scintillation detector. Diffraction intensity was measured between 4 and 80°, with a 2θ step of 0.02° and a counting time of 9 s per point. The band gap energy of the codoped material was established by UV–visible light DRS using a scanning Ocean Optics USB2000+F0009 UV-vis spectrophotometer, which was used in diffuse reflectance mode (maximal resolution, ± 2 nm). Reflectance mode studies were performed with the aid of a R400-7-UV/Vis reflection/backscattering probe [18,19]. Thereafter, optical band gap (E_g in eV) were estimated by feeding the Equation (2) with the respective wavelength onset (λ_{onset} in nm) values [20].

$$E_g = 1240 \text{ eV} \cdot \text{nm} / \lambda_{\text{onset}} \quad (2)$$

2.2. Solutions

The as-prepared codoped material was evaluated by the commercial acid blue BR dye degradation, that was supplied by PCL S.A. de C.V. (Mexico), which molecular weight is 678.68 g mol^{-1} , $\text{C}_{32}\text{H}_{28}\text{N}_2\text{Na}_2\text{O}_8\text{S}_2$ (see Table 1). The dye solutions were prepared with ultrapure water from a Millipore Milli-Q system (resistivity $> 18 \text{ M}\Omega \text{ cm}$, 25°C). The background electrolyte was introduced as Na_2SO_4 , of analytical grade, purchased from Karal. The solution's pH was adjusted to 3.0 with analytical grade H_2SO_4 , supplied by Merck. Solvents and other chemicals were either of analytical or HPLC grade, purchased from Panreac and Sigma-Aldrich.

2.3. Arrangement of photoelectrochemical system

The experiments were carried out in a stirred tank cell at laboratory scale of 200 mL. In all assays, the solution was vigorously stirred with a magnetic bar at 500 rpm in order to mix the dye and transport its mass between the catalyst and the BDD surface, obtaining with this stirring a flow in the turbulent regime (Reynolds number = 5845). The electrodes were a 5 cm² BDD thin film, purchased from MetakemTM (Germany), and 5 cm² Pt purchased from ElectrochemTM. The inter-electrode gap was of about 2.5 cm. Cyclic voltammetry curve was already reported in previous study [21]. Solutions with 50 mgL⁻¹ of acid blue dye BR in 0.5 mM Na₂SO₄ were degraded at pH 3.0 by coupled EO-BDD/TiO₂-Fe-N. The influence of the current applied between 125 and 280 Am⁻² was provided by a BK precision of 1627A power supply. UV light with $\lambda = 365$ nm and an intensity of 75 mW·cm⁻² were used to illuminate the system, provided by UVP Inc, as shown in Fig. 1.

2.4. Analytical procedures

The decolorization of dye solutions followed from their absorbance (A) decay at the maximum wavelength in the visible region of $\lambda_{\max} = 612$ nm for acid blue dye BR using a GBC-Cintra 1010 UV-VIS spectrophotometer. The percentage of color removal or decolorization efficiency was calculated by Equation (3) [22]:

$$\%Color \cdot removal = \frac{A_0 - A_t}{A_0} \times 100$$

(3)

Where A_0 and A_t are the initial and final absorbances at times 0 and t, respectively, at $\lambda_{\max} = 612$ nm.

The acid blue dye BR concentration abatement was monitored by reversed-phase high-performance liquid chromatography (HPLC) using an Agilent 1260 Infinity LC, fitted with an Agilent Eclipse C18 PAH reverse phase (250 mm × 4.6 mm 3 mm particle size), and

coupled with an Agilent G4212B diode array detector set at $\lambda = 226$ nm. Aliquots of 20 μL were injected into the LC upon elution of a 30:30:40 (v/v), $\text{CH}_3\text{OH}:\text{H}_2\text{O}:\text{CH}_3\text{CN}$ mixture was eluted at 0.8 mLmin^{-1} as mobile phase. The chromatograms displayed a peak for acid blue dye BR anion with a retention time (t_r) of 2.905 min [23].

Results and discussion

3.1. Characterization of $\text{TiO}_2\text{-Fe-N}$

It has been indicated that the incorporation of additives to TiO_2 had a suppressive effect on the crystal growth of the TiO_2 , since the additives hindered contact between TiO_2 particles and inhibited crystal growth during heat treatment [24]. It is possible to achieve a crystallinity after calcination process that is due to grain growth, which is a consequence of the increase of atomic mobility, thermally endorsed crystallite growth [25,26]; what is shown on FE-SEM images of the modified photocatalysts 0.5 wt% Fe-N codoped TiO_2 nanoparticles (Fig. 2a). The shape of titania Degussa P25-particles is generally spherical and quite stable; the pristine TiO_2 powder consists of relatively smaller and agglomerated powder particles (Fig. 2b), presenting an average size of 28 nm, value similar to other report [27]. According to the Fig. 2a, the 0.5 wt% Fe-N codoped TiO_2 nanoparticles were larger than TiO_2 Degussa P25. In addition, it can be seen that the 0.5 wt% Fe-N codoped TiO_2 powders consist of nano-sized agglomerated crystals, reaching up to 100 nm. In order to establish the achievement of the targeted chemical composition in the synthesized powders, the TiO_2 Degussa P25 nanoparticles and 0.5 wt% Fe-N codoped TiO_2 were examined by EDX, (Fig. 3a.), where we can observe the presence of titanium and no impurities and reaction products were observed in the samples.

We performed a BET analysis in order to determine the specific surface area of the TiO₂-Fe-N. Fig. 3b shows the N₂ adsorption-desorption isotherm, assuming a linear transformation of the BET values, which do not exhibit hysteresis, leading to the specific surface area 8.56 m² g⁻¹, compared with 52 m² g⁻¹ that is reported in the literature for Degussa P25 [27,28]. Textural properties revealed the value of pore volume as 0.014 cm³ g⁻¹ to TiO₂-Fe-N and 0.18 cm³ g⁻¹ for Degussa P25 [27]. Related to the pore size, a value of 5.7 nm was obtained for TiO₂-Fe-N codoped material compared to 13.7 nm in the case of Degussa P25 [27].

Fig 4. shows the XRD characterization of TiO₂-Fe-N material and pure TiO₂ nanoparticles. The peaks at $2\theta = 25.50^\circ$, 37.27° , 48.6° , 54.90° , 55.00° and 63.51° corresponding to the anatase TiO₂ phase in all the samples. All the prepared samples formed a crystalline structure and the XRD patterns of the particles were quite similar. In the case of TiO₂-Fe-N, no new peak corresponding to the incorporation of any impurity was observed. This information confirms that iron doping on titanium is carried out without changing the structure and there is only a small change in the lattice parameters of the TiO₂:Fe nanoparticles at the a-axis and c-axis in comparison with pure TiO₂ because of the doping process and the concentration of low dopant (iron atoms) in TiO₂ nanoparticles.

On the other hand, the average crystal size of the modified TiO₂-Fe-N nanoparticles was evaluated from

the line broadening of the peak (101) using the Scherrer equation [29]:

$$D = \frac{K\lambda}{\beta \cos \Theta}$$

(4)

Where, D is the average crystallite size (nm), K is the particle shape factor and taken as 0.89, λ is the X-ray wavelength corresponding to the Cu-K α irradiation, and it is the calibrated half-intensity width of the selected diffraction peak (degrees), that is, the diffraction angle. In the case of TiO₂-Fe-N the average crystal size is 29 nm.

The vibratory spectra of the structure by means of Raman spectroscopy which allows distinguishing the difference between the TiO₂-Fe-N and Degussa P25, in order to investigate the influence of Fe and N doping. Raman scattering is a technique for detecting the incorporation of dopants and the resulted defects. The major crystalline phase detected in the samples is anatase, and the sample after doping with iron-nitrogen shows amounts of rutile and anatase phases. A study of the structure in titania (Degussa P25) carried out by [30], reveals multiphasic material consisting crystalline phases anatase and rutile in the approximate proportions 80/20, and a small amount of amorphous phase. The photocatalytic activity of Degussa P25 has been given in terms of the enhancement in the magnitude of the space-charge potential, which is created by contact between the different phases.

The structural characteristics and phase composition of the Degussa P25 in comparison with TiO₂-Fe-N were further investigated by Raman spectroscopy (Fig. 5a). The titania Degussa P25 sample exhibits the characteristic Raman active phonon of the anatase phase: 516 cm⁻¹ (A_{1g}⁺ B_{1g}), 396 cm⁻¹ (B_{1g}), and 144, 197, 638 cm⁻¹ (E_g). Further increase of the calcination temperature for TiO₂-Fe-N resulted in the growth of the rutile phase, with three signals: multi-phonon (230 cm⁻¹), E_g 445 cm⁻¹ and A_{1g} 610 cm⁻¹. E_g B_{1g} and A_{1g} are caused by symmetric stretching, bending and antisymmetric O-Ti-O, respectively [31].

The relative anatase/rutile ratio has been determined from the integrated areas of the Raman analysis of the anatase 396 cm^{-1} and rutile 440 cm^{-1} bands, and values of Degussa P25 and $\text{TiO}_2\text{-Fe-N}$, respectively. The fact that the anatase and rutile structure for the Fe-doped TiO_2 nanoparticles is preserved indicates that the iron dopant is substitutionally interposed in the TiO_2 frame-work replacing Ti^{4+} cation [32,33].

Respecting the dopant nitrogen, we must consider 3 main factors to explain its effect: the synthesis conditions adopted, the annealing made to the sample, and the quantity of the dopant urea species in Degussa P25. If the factors mentioned above are ignored, the simple doping will provide only two possibilities: that the nitrogen can act as a recombination center, or that it can promote the recombination because of the generation of oxygen vacancies. It is difficult to assign an optimal value to the nitrogen dopant species concentration and to calculate the real quantity of nitrogen associated to the titania lattice, which never matches with the nominal estimation. Since the thermal treatment is at $500\text{ }^\circ\text{C}$, it can be inferred that the generated vacancies are oxygen ones, because it is difficult to attach nitrogen to the lattice [5].

UV-Vis diffuse reflectance spectra were recorded to determine the effect of metal doping on the TiO_2 absorption edge (Fig. 5b). As can be seen, the E_g value for TiO_2 Degussa P25 was 3.3 eV at $\lambda = 375\text{ nm}$, similar to the value given in different reports [6,34,35]. However, an increase in the absorbance capacity at approximately $\lambda = 420\text{ nm}$ was observed in the case of the sample doped with the Fe-N amount, producing the decrease in the E_g value, close to 2.9 eV . This behavior can be attributed to the interfacial charge transfer from Fe^{3+} to the conduction band of Ti(IV) and partially to the $4\text{A}2\text{g} \rightarrow 4\text{T}1\text{g}$ transition band of Fe^{3+} [36].

3.2. Photoelectrocatalysis acid blue dye BR degradation

The degradation of acid blue dye BR solutions was carried out by EO. In this electrochemical technique, pollutants are mainly degraded by the action of adsorbed $\cdot\text{OH}$ formed as intermediaries at the surface of a high O_2 -overvoltage anode from water oxidation reaction (1). Free radical $\cdot\text{OH}$ is a non-selective, strong oxidizing agent, able to react with the most organic compounds until their total mineralization, i.e. their conversion into CO_2 [37,38]. Recent investigations have confirmed that the sp^3 (diamond)/ sp^2 (graphite) ratio has a key role in the electrochemical properties of BDD electrodes. The most relevant result supposes that the EO mechanism is strongly influenced by the BDD characteristics; particularly the ratio diamond/graphite carbon. High graphite content favors direct oxidation of the pollutant on the electrode surface and it leads to the formation of many intermediates. On contrary, high diamond content seems to favor the complete oxidation of the organic to CO_2 [39,40].

The decay in color of dyes wastewater during treatment by advanced oxidation processes is usually monitored from the decolorization efficiency or percentage of color removal determined from UV-vis spectrophotometry measurements [3,35,37]. So, acid blue dye BR solutions at initial concentration of 50 mgL^{-1} treated by EO with BDD anodes were progressively degraded with prolonging electrolysis time up to 60 min, according to the gradual decay observed for the color.

The current density is a key parameter in EO with BDD anodes, because it regulates the amount of oxidant BDD ($\cdot\text{OH}$) produced by reaction (1) [41]. The influence of this independent variable on the decolorization of acid blue dye BR solutions is illustrated in Fig. 6. As it can be seen, an increase in the applied current led to higher degradation rate, at

60 min of degradation the color removal for 50 mgL⁻¹ dye was only of 15% at 125 Am⁻² (■), whereas for 280 Am⁻² (●) reached around 25% for the same treatment time. The higher degradation rate with the increasing current applied can be simply associated with the concomitant acceleration of reaction (1), thereby generating larger quantities of BDD (·OH) that destroy further and quickly the organic compounds [42].

In the same figure, it is also possible to observe the changes in the color as a function of the oxidant dosage during the treatment of acid blue dye BR solutions with EO and photocatalysis, using the TiO₂-Fe-N material. As it also can be observed, both technologies are able to decrease significantly the organic quantity of the synthetic waste, although the performances observed are completely different [43,44].

When EO is coupled with the photocatalysis using TiO₂-Fe-N (via photoelectrocatalysis), the performance in terms of color removal is different to that obtained working with the individual processes of EO or photocatalysis[45], as it can be seen in Fig. 6. The degradation of the acid blue dye BR solution was carried out by anodic oxidation combined with photocatalysis, TiO₂-Fe-N, both advanced oxidation processes, produce efficiently free radicals ·OH. It is worth noticing that the pH was constant during all the experiments.

With the objective of comparing the photoactivity of both TiO₂-N-Fe and Degussa P25 TiO₂ photocatalysts, different tests were performed using 1 gL⁻¹ of each catalyst in a medium illuminated with UV light to degrade 50 mgL⁻¹ of the acid blue BR dye. The results depicted in Fig. 6 indicate that only 12% of color removal is achieved when commercial TiO₂ is used (x), while the catalyst TiO₂-Fe-N (+) favors higher degradation

yield, close to 29%, which highlights that the synthesized material is more effective for color removal under the conditions analyzed in this work.

Additionally, in order to evaluate the abatement of acid blue dye BR concentration, reversed-phase liquid chromatography tests were performed. These chromatograms exhibited a well-defined peak for this compound at $t_r = 2.905$ min (Fig. 7a). As shown in Fig. 7b, under EO process at 125 Am^{-2} current density (■), it is possible to reduce the dye concentration by 30%. When the current was increased to 280 Am^{-2} , it is possible to observe an important increase in the degradation rate, where in the first 60 min the process achieved 77% of degradation (●). For the case with the coupled process EO-BDD/Photocatalysis $\text{TiO}_2\text{-Fe-N}$, when 125 Am^{-2} is applied, an important degradation is obtained, only in the first 60 minutes the dye degraded to 85% (▼). The most successful result is obtained when 280 Am^{-2} is carried out, achieving 99% of acid blue dye BR degradation (◆). A gradual increase in acid blue dye BR removal is carried out by the rising current from 125 Am^{-2} to 280 Am^{-2} in both cases. This enhancement of the degradation can be associated with a faster destruction of pollutants by the increase in the rate of reaction (5) to produce more quantity of $\cdot\text{OH}$.



3.3. Identification of short-linear aliphatic carboxylic acids

The 50 mgL^{-1} acid blue dye BR solutions were analyzed at regular times by ion-exclusion HPLC during their electrolysis at 280 Am^{-2} by the EO-BDD/Photocatalysis $\text{TiO}_2\text{-Fe-N}$ for 300 min to identify and quantify the final short-linear aliphatic carboxylic acids produced [11,37], as can be seen in Fig. 8. These chromatograms displayed well-defined peaks

related to (◆) oxalic, (●) maleic, (■) glyoxylic, and (▲) glycolic acids. The former four acids can proceed from the cleavage of the rings of the dye, and they subsequently lead to complete mineralization with further treatment time [46,47]. The evolution of the most significant acids was carried out as follows: Glyoxylic and glycolic acids were always accumulated in very low concentrations ($<3 \text{ mgL}^{-1}$), tending to disappear from the medium after 60 min. In the case of maleic acid, there was an accumulation close to 1.3 mgL^{-1} in the first 60 min, as the oxidation evolves. Finally, it was observed that the concentration of oxalic acid was increased around 3 mgL^{-1} in first hour of treatment.

3.4. Synergistic analysis

It was interesting to know the synergistic effect between the EO (*Process-1*) and photocatalysis (*Process-2*). This synergistic analysis was evaluated by relating the rate constants (k) of the individual and combined processes through Equation (6), as reported by several authors [48,49]:

$$\% \text{ Synergy} = 1 - \frac{k_{\text{Process-1}} + k_{\text{Process-2}}}{k_{\text{Combined-processes}}} \times 100 \quad (6)$$

Then, Equation (7) was obtained rearranging the values of k corresponding to the processes applied for the treatment of acid blue dye BR solutions.

$$\% \text{ Synergy} = 1 - \frac{k_{\text{EO-BDD}} + k_{\text{TiO}_2\text{-Fe-N}}}{k_{\text{EO-BDD/TiO}_2\text{-Fe-N}}} \times 100 \quad (7)$$

Where $k_{\text{EO-BDD}}$ and $k_{\text{TiO}_2\text{-Fe-N}}$ are the kinetic constants of color removal via EO with BDD anode and via photocatalysis using the synthesized catalyst, while the $k_{\text{EO-BDD/TiO}_2\text{-Fe-N}}$ is the kinetic constant of color removal of the photoelectrocatalytic treatment.

Therefore, the pseudo-first order rate constants were calculated, as well as the regression coefficients (R^2) for both technologies. These values are shown on Table 2.

From the kinetic constants it was possible to quantify the synergy between the processes. There appears to be a synergistic effect between EO and photocatalysis $\text{TiO}_2\text{-Fe-N}$, since the rate constants of the combined processes ($k_{\text{EO-BDD/TiO}_2\text{-Fe-N}}$) are greater than the sum of the rate constants of the individual processes ($k_{\text{EO-BDD}} + k_{\text{TiO}_2\text{-Fe-N}}$) [48].

Regarding the relative contribution of individual oxidation technologies to the global color removal the effect of each individual process was determined using Equations (8) and (9):

$$\%EO - BDD = \frac{k_{EO-BDD}}{k_{EO-BDD / \text{TiO}_2 - \text{Fe} - \text{N}}} \times 100$$

(8)

$$\% \text{TiO}_2 - \text{Fe} - \text{N} = \frac{k_{\text{TiO}_2 - \text{Fe} - \text{N}}}{k_{EO-BDD / \text{TiO}_2 - \text{Fe} - \text{N}}} \times 100 \quad (9)$$

Fig. 9 shows the synergistic effects during the color removal of acid blue dye BR via single EO-BDD, single $\text{TiO}_2\text{-Fe-N}$ and EO-BDD/Photocatalysis $\text{TiO}_2\text{-Fe-N}$ at 125 and 280 Am^{-2} , respectively. In Fig. 9, it was also depicted that EO-BDD/ $\text{TiO}_2\text{-Fe-N}$ at 280 Am^{-2} allowed 71.3% of synergy, while EO-BDD/ $\text{TiO}_2\text{-Fe-N}$ at 125 Am^{-2} reached 17.9%. Therefore, this effect was most evident operating at the highest current density; it was 4 fold higher than at 125 Am^{-2} . This means that there was a beneficial effect of coupling EO with the photocatalytic process in both cases.

The fast recombination of the electron-hole pairs formed is avoided in photoelectrocatalysis by applying an external bias potential to the photocatalyst that extracts the photogenerated

electrons up to the cathode of the electrolytic cell, improving the production of hydroxyl radicals generated by the oxidation of water through the holes at the TiO₂ valence band. [50,51].

3.5. Energy consumption

One way to evaluate the energy input of the different processes is through estimation of the parameter Electric Energy per Order (E_{EO}) that relates the kinetics of each treatment and its energy consumption to the color removal [50]. The E_{EO} is defined as the electric energy required to degrade a concentration of pollutant by one order of magnitude (90%) in a unit volume of aqueous solution [11]. Equation (10) shows the expression used to calculate the E_{EO} in kWhm⁻³order⁻¹, where the values of color decay are used because these values were adequately fitted to a pseudo-first order kinetic expression [50,52].

$$E_{EO} = \frac{P_{el}}{V \cdot \log\left(\frac{color_0}{color_f}\right)}$$

(10)

Equation (11) is obtained rearranging values:

$$E_{EO} = \frac{P_{el}}{V \cdot 0.434 \cdot k \cdot 60}$$

(11)

P_{el} is the electric power (kW), t is time (h), V is the reaction volume (m³), k is the pseudo-first order kinetic constant (min⁻¹) determined previously for color removal.

Fig. 10 shows that the EO process using a current density of 125 Am⁻² required the lowest energy consumption of 23.76 kWhm⁻³order⁻¹, while EO with 280 Am⁻² required almost 3 fold E_{EO} (67.55 kWhm⁻³order⁻¹); those values are in agreement with other reports of

electrochemical treatment of dyes and other compounds [11,52]. On the other hand, photocatalysis using $\text{TiO}_2\text{-Fe-N}$ required the highest energy consumption reaching a value of $984.62 \text{ kWhm}^{-3} \text{ order}^{-1}$, mainly due to the electric power consumed by the lamp ($2.0 \times 10^{-2} \text{ kW}$) compared to EO ($1.5 \times 10^{-3} - 3.7 \times 10^{-4} \text{ kW}$).

The coupling of EO-BDD with photocatalysis using $\text{TiO}_2\text{-Fe-N}$ at 280 Am^{-2} provided a decrease in the value of E_{EO} around 3 fold lower ($140.18 \text{ kWhm}^{-3} \text{ order}^{-1}$) than the value obtained with EO-BDD/ $\text{TiO}_2\text{-Fe-N}$ at 125 Am^{-2} ($465.26 \text{ kWhm}^{-3} \text{ order}^{-1}$). This behavior was due to the high values of kinetic constants obtained at 280 Am^{-2} via photoelectrocatalysis.

4. Conclusions

At the beginning of this investigation we raised two important questions, the first was if the degradation of dye blue acid dye BR could be successfully achieved using the catalyst $\text{TiO}_2\text{-Fe-N}$ coupled with BDD anode. In this sense, the answer is positive, since the results show that the coupled process provides an improvement of one order of magnitude in relation to the others. The second question was related to the effect of operation variables such as current density. Here, the results are evident, since as it was found, a gradual increase in the intensity of the current considerably improves the degradation of the dye, and a greater amount of oxidizing species is produced. Regarding synergy effect, both processes resulted positive. However, at 280 Am^{-2} this effect was more evident than at less current density.

Regarding energy consumption, EO processes allowed a lower E_{EO} in comparison to photoelectrocatalytic processes. However, when coupling the EO-BDD and the photocatalysis $\text{TiO}_2\text{-Fe-N}$, kinetic constant increased.

In the light of these results, our perspectives will now focus on the study of the coupled mechanism; as well, we will make an evaluation of the possible routes of degradation of the dye studied.

Acknowledgements

The authors thank the PRODEP Program (PRODEP-UGTO-PTC-472 and PRODEP 2015 UGTO-PTC-457) of UGTO under the Project 007/2015 (Convocatoria Institucional para Fortalecer la Excelencia Académica 2015), and the Project 778/2016 (Convocatoria Institucional de Apoyo a la Investigación Científica 2016-2017) is acknowledged. Authors thank Guanajuato University-CONACYT National Laboratory for SEM-EDX analysis. Financial support from the Spanish Ministry of Economy and Competitiveness in projects CTM2015-69845-R and CTQ2015-66078-R (MINECO/FEDER, UE) is gratefully acknowledged. C. J. Escudero thanks CONACYT-CONCYTEG for the postgraduate research grant (230713/383108) from Mexico.

References

- [1] V. Binas, D. Venieri, D. Kotzias, G. Kiriakidis, Modified TiO₂ based photocatalysts for improved air and health quality. *J. Materiomics*. 3 (2017) 3-16.
- [2] R. Daghrir, P. Drogui, D. Robert, Modified TiO₂ for environmental photocatalytic applications: A review. *Ind. Eng. Chem. Res.* 52 (2013) 3581-3599.
- [3] M. Khairy, W. Zakaria, Effect of metal-doping of TiO₂ nanoparticles on their photocatalytic activities toward removal of organic dyes. *J. Egypt. J. Pet.* 23 (2014), 419-426.

- [4] S. Wang, X. Cheng, Solar photocatalytic degradation of typical indoor air pollutant using TiO₂ thin film codoped with iron (III) and nitrogen. *J. Spectrosc.* 215 (2015) [Article ID 259829].
- [5] T.C. Jagadale, S.P. Takale, R.S. Sonawane, H.M. Joshi, S.I. Patil, B.B. Kale, S.B. Ogale, N-doped TiO₂ nanoparticle based visible light photocatalyst by modified peroxide sol-gel method. *J. Phys. Chem. C.* 112 (2008) 14595-14602.
- [6] F. Azizi, F. Molani, Effects of N Doping on structure and improvement photocatalytic properties of anatase TiO₂ nanoparticles. *J. Nanostruct.* 6 (2016) 58-63.
- [7] A.O. Ibhadon, P. Fitzpatrick, Heterogeneous photocatalysis: Recent advances and applications. *Catalysts.* 3 (2013) 189-218.
- [8] I. Sires, E. Brillas, M.A. Oturan, M.A. Rodrigo, M. Panizza, Electrochemical advanced oxidation processes: Today and tomorrow. A review. *Environ. Sci. Pollut. Res.* 21 (2014) 8336-8367.
- [9] C.A. Martínez-Huitle, M.A. Rodrigo, I. Sires, O. Scialdone, Single and coupled electrochemical processes and reactors for the abatement of organic water pollutants: a critical review. *Chem. Rev.* 115 (2015) 13362-13407.
- [10] C. Espinoza, J. Romero, L. Villegas, L. Cornejo-Ponce, R. Salazar, Mineralization of the textile dye acid yellow 42 by solar photoelectro-Fenton in a lab-pilot plant. *J. Hazard. Mater.* 319 (2016) 24-33.

- [11] C.J. Escudero, O. Iglesias, S. Dominguez, M.J. Rivero, I. Ortiz, Performance of electrochemical oxidation and photocatalysis in terms of kinetics and energy consumption. New insights into the p-cresol. *J. Environ. Manag.* 195 (2016) 117-124.
- [12] E. Bocos, N. Oturan, M.A. Sanromán, M.A. Oturan, Elimination of radiocontrast agent Diatrizoic acid from water by electrochemical advanced oxidation: Kinetics study, mechanism and mineralization pathway. *J. Electroanal. Chem.* 772 (2016) 1-8.
- [13] H. Zazou, N. Oturan, M. Sönmez-Çelebi, M. Hamdani, M.A. Oturan, Mineralization of chlorobenzene in aqueous medium by anodic oxidation and electro-Fenton processes using Pt or BDD anode and carbon felt cathode. *J. Electroanal. Chem.* 774 (2016) 22-30.
- [14] A. Anglada, A.M. Urtiaga, I. Ortiz, Contributions of electrochemical oxidation to wastewater treatment: Fundamentals and review of applications. *J. Chem. Tech. Biotech.* 84 (2009) 1747-1755.
- [15] D.R. Da Silva, M.B. Ferreira, C.N. Brito, S. Ferro, C.A. Martínez-Huitle, A. De Battisti, Anodic oxidation of tartaric acid at different electrode materials. *Curr. Org. Chem.* 16(17) (2012) 1951-1956.
- [16] S. Ferro, C.A. Martínez-Huitle, A. De Battisti, Electrooxidation of oxalic acid at different electrode materials. *J. Appl. Electrochem.* 40 (2010) 1779-1787.
- [17] F.J. González-Fuentes, J. Manríquez, L.A. Godínez, A. Escarpa, S. Mendoza, Electrochemical Analysis of Acrylamide Using Screen-Printed Carboxylated Single-Walled Carbon Nanotube Electrodes. *Electroanalysis.* 26 (2014) 1039-1044.

- [18] U. López-García, O.A. Castellanos, L.A. Godínez, J. Manríquez, Electrophoretically-Assisted Deposition of Mesoporphyrin IX on Nano particulate TiO₂ Films for Constructing Efficient Dye-Sensitized Solar Cells. *J. Electrochem. Soc.* 158 (2011) F100-F105.
- [19] J.C. Baltazar-Vera, R. Fuentes-Ramírez, E. Bustos, G. Carreño-Aguilera, J. Manríquez, Disperse red 1 and reactive red 2 – modified nanoparticulate TiO₂ films as photoanodes for studying photovoltaic properties of textile azo dyes. *J. Photochem. Photobiol. A.* 307 (2015) 68-78.
- [20] A. Hagfeldt, M. Grätzel, Light-Induced Redox Reactions in Nano crystalline Systems. *Chem. Rev.* 95 (1995) 49-68.
- [21] F. Espinola-Portilla, R. Navarro-Mendoza, S. Gutiérrez-Granados, U. Morales-Muñoz, E. Brillas-Coso, J.M. Peralta-Hernández, A simple process for the deposition of TiO₂ onto BDD by electrophoresis and its application to the photoelectrocatalysis of Acid Blue 80 dye. *J. Electroanal. Chem.* 802 (2017) 57-63.
- [22] H. Jalife-Jacobo, R. Feria-Reyes, O. Serrano-Torres, S. Gutiérrez-Granados, J.M. Peralta-Hernández, Diazo dye Congo Red degradation using a Boron-doped diamond anode: An experimental study on the effect of supporting electrolytes. *J. Hazard. Mater.* 319 (2016) 78-83.
- [23] A. Bedolla-Guzman, I. Sirés, A. Thiam, J.M. Peralta-Hernández, S. Gutiérrez-Granados, E. Brillas, Application of anodic oxidation, electro-Fenton and UVA photoelectro-Fenton to decolorize and mineralize acidic solutions of Reactive Yellow 160 azo dye. *Electrochim. Acta.* 206 (2016) 307-316.

- [24] J. Yu, J.C. Yu, X. Zhao, The effect of SiO₂ addition on the grain size and photocatalytic activity of TiO₂ thin films. *J. Sol-Gel. Sci. Technol.* 24 (2002) 95-103.
- [25] Y.F. Chen, C.Y. Lee, M.Y. Yeng, H.T. Chiu, The Effect of Calcination Temperature on the Crystallinity of TiO₂ Nano powder. *J. Crystal Growth.* 247 (2003) 363-370.
- [26] Y.S. Chang, The Effects of Heat Treatment on the Crystallinity and Luminescence Properties of YInGe₂O₇ Doped with Eu³⁺ Ions, *J. Electronic. Mat.* 37 (2008) 1024-1028.
- [27] K.J.A. Raj, B. Viswanathan. Effect of surface area, pore volume and particle size of P25 titania on the phase transformation of anatase to rutile. *Indian J. Chem.* 48A (2009) 1378-1382.
- [28] J. Choi, H. Park, M.R. Hoffmann, Effects of single metal ion doping on the visible-light photoreactivity of TiO₂. *J. Phys. Chem. C.* 114 (2010) 783-792.
- [29] S. Mirshahghassemi, J.R. Lead, Oil recovery from water under environmentally relevant conditions using magnetic nanoparticles. *Environ. Sci. Technol.* 49 (2015) 11729-11736.
- [30] R.I. Bickley, T. Gonzalez-Carreno, J.S. Lees, L. Palmisano, R.J.D. Tilley, A Structural Investigation of Titanium Dioxide Photocatalysts. *J. Solid State Chem.* 92 (1991) 178-190.
- [31] T. Huang, S. Mao, J. Yu, Z. Wen, G. Lu, J. Chen, Effects of N and F doping on structure and photocatalytic properties of anatase TiO₂ nanoparticles. *RSC Adv.* 3(37) (2013) 16657-16664.
- [32] B. Hsu, S. Chen, C. Su, Y. Li, Preparation and characterization of nanocrystalline Fe/N co-doped titania. *Ferroelectrics.* 381 (2009) 51-58.

- [33] K. Zhang, X. Wang, X. G., T. He, Y. Feng, Preparation of highly visible light active Fe-N co-doped mesoporous TiO₂ photocatalyst by fast sol-gel method. *J. Nanopart. Res.* 16 (2014) 1-9.
- [34] S. Mozia, Generation of useful hydrocarbons and hydrogen during photocatalytic decomposition of acetic acid on CuO/Rutile photocatalysts. *Int. J. Photoenergy*. 2009 (2009) [Article ID 469069].
- [35] M. Carević, N.D. Abazović, T. Savić, T.B. Novaković, M.D. Mojović, M.I. Čomor, Structural, optical and photodegradation properties of pure and Fe-doped titania nanoparticles probed using simulated Solar light. *Ceram. Int.* 42 (2016) 1521-1529.
- [36] S.Y. Mendiola-Alvarez, J.L. Guzmán-Mar, G. Turnes-Palomino, F. Maya-Alejandro, A. Hernández-Ramírez, L. Hinojosa-Reyes, UV and visible activation of Cr(III)-doped TiO₂ catalyst prepared by a microwave-assisted sol-gel method during MCPA degradation. *Environ. Sci. Pollut. Res.* 24 (2017) 12673–12682.
- [37] E. Brillas, C.A. Martínez-Huitle, Decontamination of wastewaters containing synthetic organic dyes by electrochemical methods. An updated review. *Appl. Catal. B: Environ.* 166-167 (2015) 603-643.
- [38] P. Fernández-Castro, M. Vallejo, M.F. San Román, I. Ortiz, Role and review of the determination methods of reactive oxygen species. *J. Chem. Tech. Biotech.* 90 (2015) 796-820.
- [39] S. Garcia-Segura, E.V. Dos Santos, C.A. Martínez-Huitle, Role of sp³/sp² ratio on the electrocatalytic properties of boron-doped diamond electrodes: A mini review. *Electrochem. Commun.* 59 (2015) 52-55.

- [40] D. Medeiros, P. Cañizares, C.A. Martínez-Huitle, M.A. Rodrigo, Electrochemical conversion/combustión of a model organic pollutant on BDD anode: Role of sp^3/sp^2 ratio. *Electrochem. Commun.* 47 (2014) 37-40.
- [41] D.M. De Araujo, S. Cotillas, C. Sáez, P. Cañizares, C.A. Martínez-Huitle, M.A. Rodrigo, Activation by light irradiation of oxidants electrochemically generated during Rhodamine B elimination. *J. Electroanal. Chem.* 757 (2015) 144-149.
- [42] C. Ramírez, A. Saldaña, B. Hernández, R. Acero, R. Guerra, S. Garcia-Segura, E. Brillas, J.M. Peralta-Hernández, Electrochemical oxidation of methyl orange azo dye at pilot flow plant using BDD technology. *J. Ind. Eng. Chem.* 19 (2013) 571-579.
- [43] J.M. Peralta-Hernández, J. Manríquez, Y. Meas-Vong, F.J. Rodríguez, T.W. Chapman, M.I. Maldonado, L.A. Godínez, Photocatalytic properties of nano-structured TiO_2 -carbon films obtained by means of electrophoretic deposition. *J. Hazard. Mater.* 147 (2007) 588-593.
- [44] J.M. Peralta-Hernández, C. De la Rosa-Juárez, V. Buzo-Muñoz, J. Paramo-Vargas, P. Cañizares-Cañizares, M.A. Rodrigo-Rodrigo, Synergism between anodic oxidation with diamond anodes and heterogeneous catalytic photolysis for the treatment of pharmaceutical pollutants. *Sust. Environ. Res.* 26 (2016) 70-75.
- [45] S. Cotillas, M.J. De Vidales, J. Llanos, C. Sáez, P. Cañizares, M.A. Rodrigo, Electrolytic and electro-irradiated processes with diamond anodes for the oxidation of persistent pollutants and disinfection of urban treated wastewater. *J. Hazard. Mater.* 319 (2016) 93-101.

- [46] P. Cañizares, J. García-Gómez, J. Lobato, M.A. Rodrigo, Electrochemical oxidation of aqueous carboxylic acid wastes using diamond thin-film electrodes. *Ind Eng Chem Res.* 42(5) (2003) 956-962.
- [47] E. Weiss, K. Groenen-Serrano, A. Savall, C. Comninellis, A kinetic study of the electrochemical oxidation of maleic acid on boron doped diamond. *J. Appl. Electrochem.* 37(41) (2007) 41-47.
- [48] C. Berberidou, I. Poulios, N.P. Xekoukoulotakis, D. Mantzavinos, Sonolytic, photocatalytic and sonophotocatalytic degradation of malachite green in aqueous solutions. *Appl. Catal. B: Environ.* 74 (2007) 63-72.
- [49] E. Bringas, J. Saiz, I. Ortiz, Kinetics of ultrasound-enhanced electrochemical oxidation of diuron on boron-doped diamond electrodes. *Chem. Eng. J.* 172 (2011) 1016-1022.
- [50] J. Carvalho, G. Garcia, M.V. Boldrin, Efficiency comparison of ozonation, photolysis, photocatalysis and photoelectrocatalysis methods in real textile wastewater decolorization. *Water Res.* 98 (2016), 39-46.
- [51] S. Garcia-Segura, E. Brillas, Applied photoelectrocatalysis on the degradation of organic pollutants in wastewaters. *J. Photochem. Photobiol. C: Photochem. Rev.* 31 (2017) 1-35.
- [52] G. Malpass, D. Miwa, D. Mortari, S. Machado, A. Motheo, Decolorisation of real textile waste using electrochemical techniques: Effect of the chloride concentration. *Water Res.* 41 (2008) 2969-2977.

Tables.

Table 1. Acid blue BR dye properties.

Table 2. Kinetics constants of the color removal for the individual and combined oxidation processes.

Figure Captions.

Figure 1. Schematic of experimental setup used. a) Reactor of borosilicate glass, b) Electrodes (anode and cathode), c) Power Supply (BK Precision), d) Stirring plate (Corning), e) UV light source.

Figure 2. Results of the FE-SEM analysis of the (a) Titania 0.5 wt% Fe-N codoped nanoparticles after thermal treatment; (b) Titania Degussa P25 spherical nanoparticles undoped.

Figure 3. (a) EDX graphic of the Titania 0.5 wt% Fe-N codoped; (b) N₂ Adsorption-Desorption Isotherm obtained codoped TiO₂-Fe-N.

Figure 4. XRD patterns of the pure TiO₂ and TiO₂-Fe-N nanoparticles, pure TiO₂ (blue line), TiO₂-Fe-N (red line). The anatase and rutile phases are identified as A and Ru, respectively.

Figure 5. (a) Raman spectra obtained for Fe-doped (red line) and un-doped (blue line) TiO₂ powders; (b) UV-vis spectra obtained for Fe-doped (red line) and un-doped (blue line) TiO₂ powders.

Figure 6. Color removal for the treatment of 200 mL of a solution of 50 mgL⁻¹ acid blue dye BR with 0.5 mM Na₂SO₄ at pH 3. Single Electrochemical oxidation (EO-BDD) (■,●).

Combined EO-BDD/Photocatalysis $\text{TiO}_2\text{-Fe-N}$ ($\blacktriangledown, \blacklozenge$). Applied current density: ($\blacksquare, \blacktriangledown$) 125 Am^{-2} and (\bullet, \blacklozenge) 280 Am^{-2} , respectively. Single photocatalysis $\text{TiO}_2\text{-Fe-N}$ (+) and TiO_2 (X). Experiments were carry out adding 1 gL^{-1} $\text{TiO}_2\text{-Fe-N}$ catalyst and using 5 cm^2 BDD electrode area. Solid lines correspond to simulated values fitted to a pseudo-first order kinetic.

Figure 7. (a) Representative chromatogram of the acid blue dye and its retention time. Change of (b) degradation dye rate obtained by single electrochemical oxidation (EO-BDD) (\blacksquare, \bullet) and by combined EO-BDD/Photocatalysis $\text{TiO}_2\text{-Fe-N}$ ($\blacktriangledown, \blacklozenge$) during the treatment of acid blue dye BR solutions. Applied current density: ($\blacksquare, \blacktriangledown$) 125 Am^{-2} and (\bullet, \blacklozenge) 280 Am^{-2} .

Figure 8. Time-course of the concentration of oxalic (\blacklozenge), maleic (\bullet), glyoxylic(\blacksquare) and glycolic (\blacktriangle) acids detected during the EO-BDD/Photocatalysis $\text{TiO}_2\text{-Fe-N}$ degradation of 200 mL of a solution of 50 mgL^{-1} acid blue BR in $0.5 \text{ mM Na}_2\text{SO}_4$ at pH 3.0 using a stirred BDD/air-diffusion tank reactor at 280 Am^{-2} .

Figure 9. Synergistic effects during the color removal of acid blue dye BR via single EO-BDD, single $\text{TiO}_2\text{-Fe-N}$ and EO-BDD/Photocatalysis $\text{TiO}_2\text{-Fe-N}$ at 125 and 280 Am^{-2} , respectively. Experimental conditions: 200 mL of acid blue dye BR 50 mgL^{-1} , solution in $0.5 \text{ mM Na}_2\text{SO}_4$ at pH 3, adding 1 gL^{-1} $\text{TiO}_2\text{-Fe-N}$ catalyst and using 5 cm^2 BDD electrode area.

Figure 10. Electrical Energy per Order (E_{EO}) estimated for the color removal applying different oxidation processes. Experimental conditions: 200 mL of acid blue dye BR 50

mgL⁻¹, solution in 0.5 mM Na₂SO₄ at pH 3, adding 1 gL⁻¹ TiO₂-Fe-N catalyst and using 5 cm² BDD electrode area.

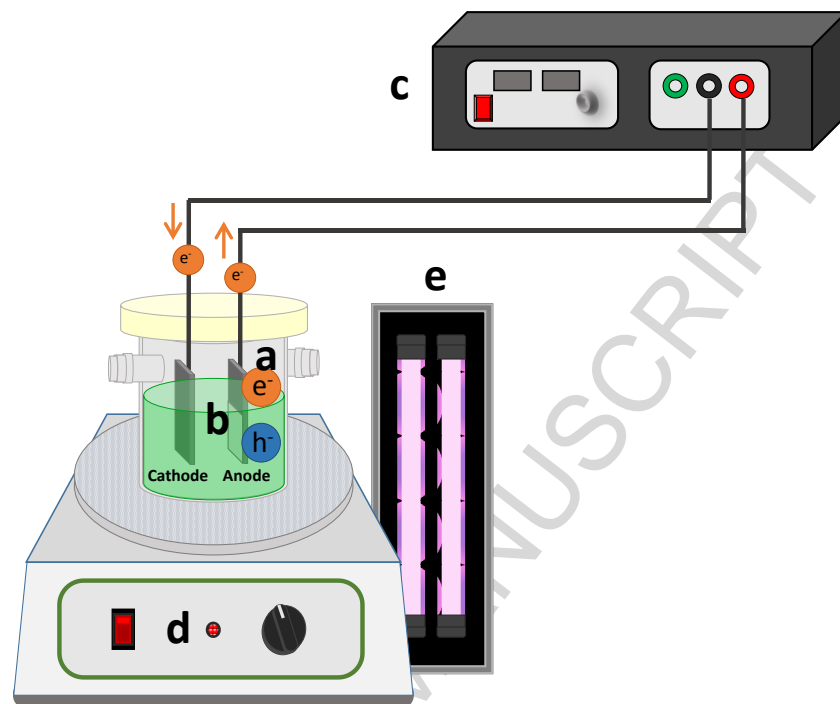
Figure 1.

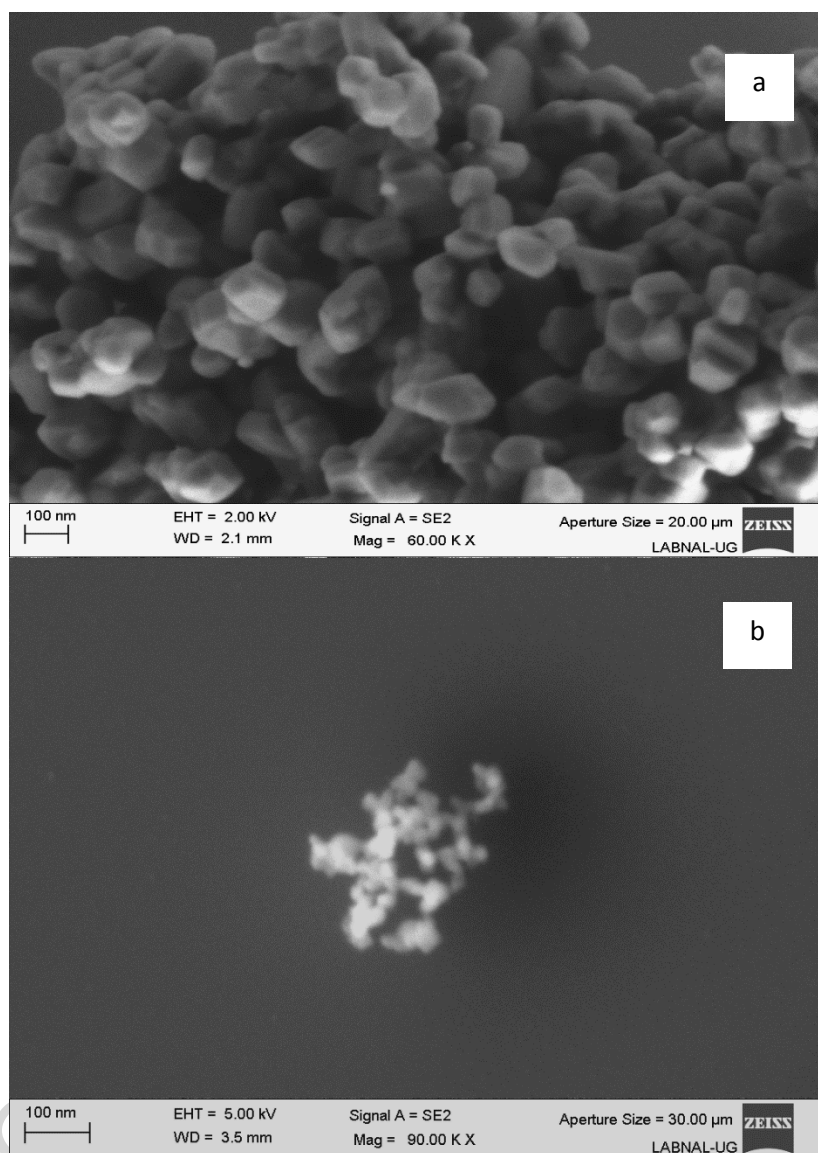
Figure 2.

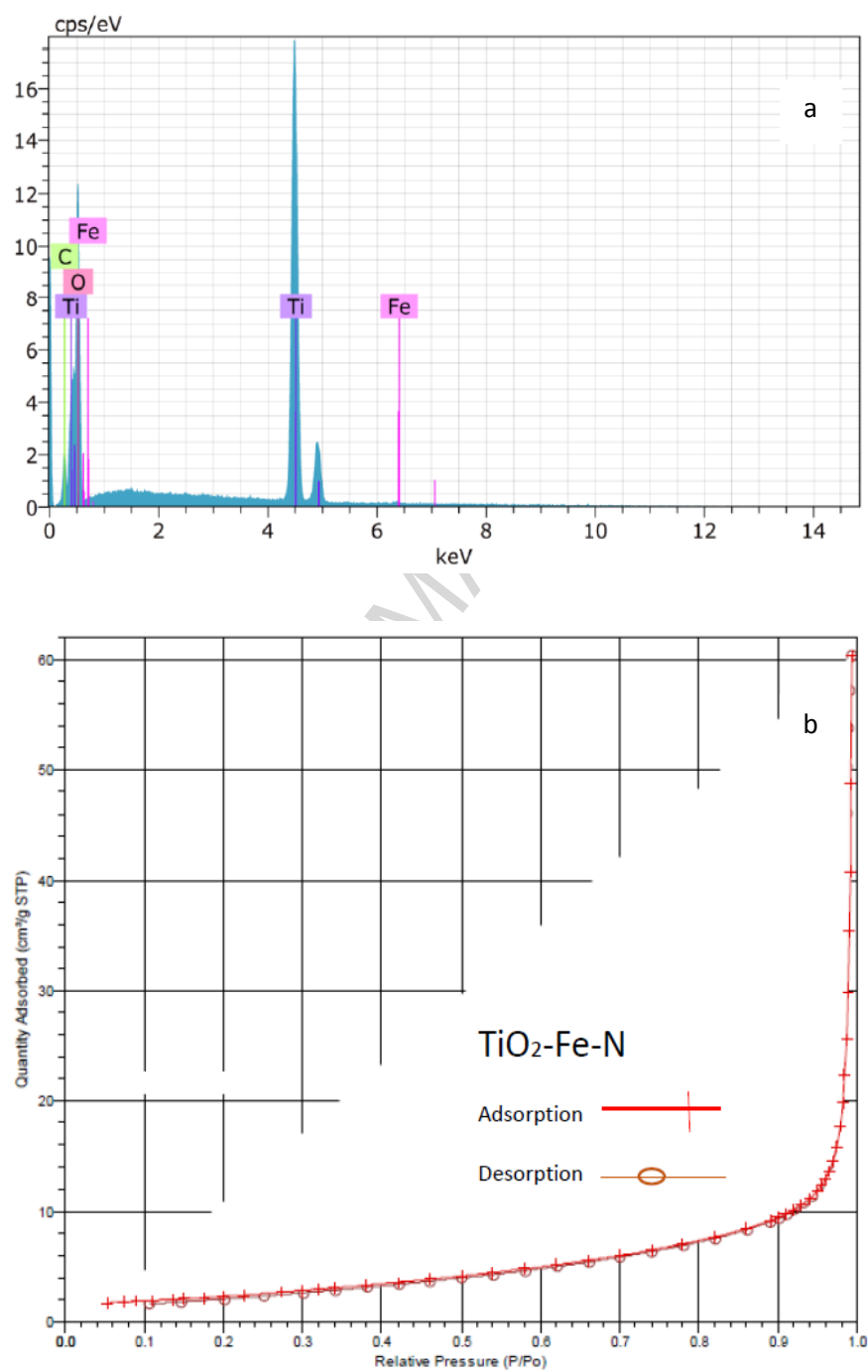
Figure 3.

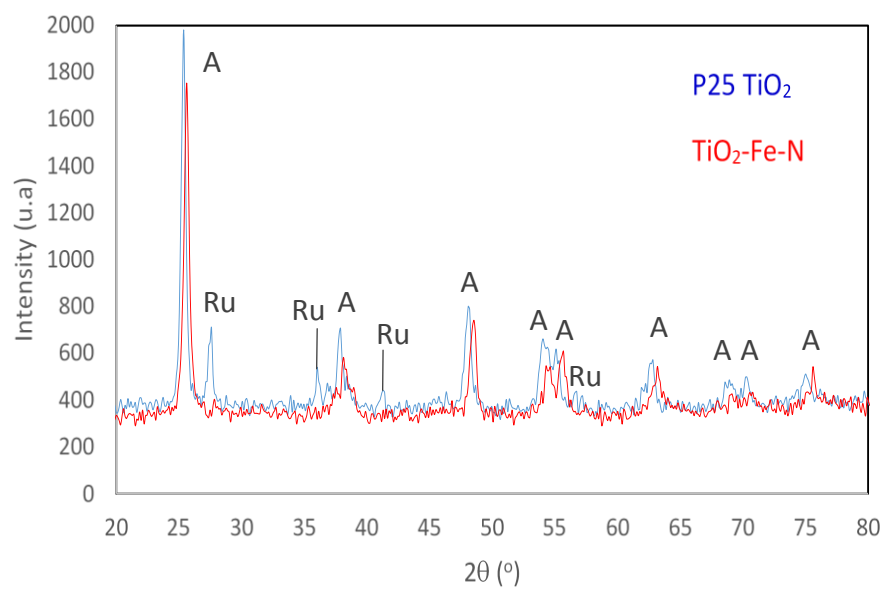
Figure 4.

Figure 5

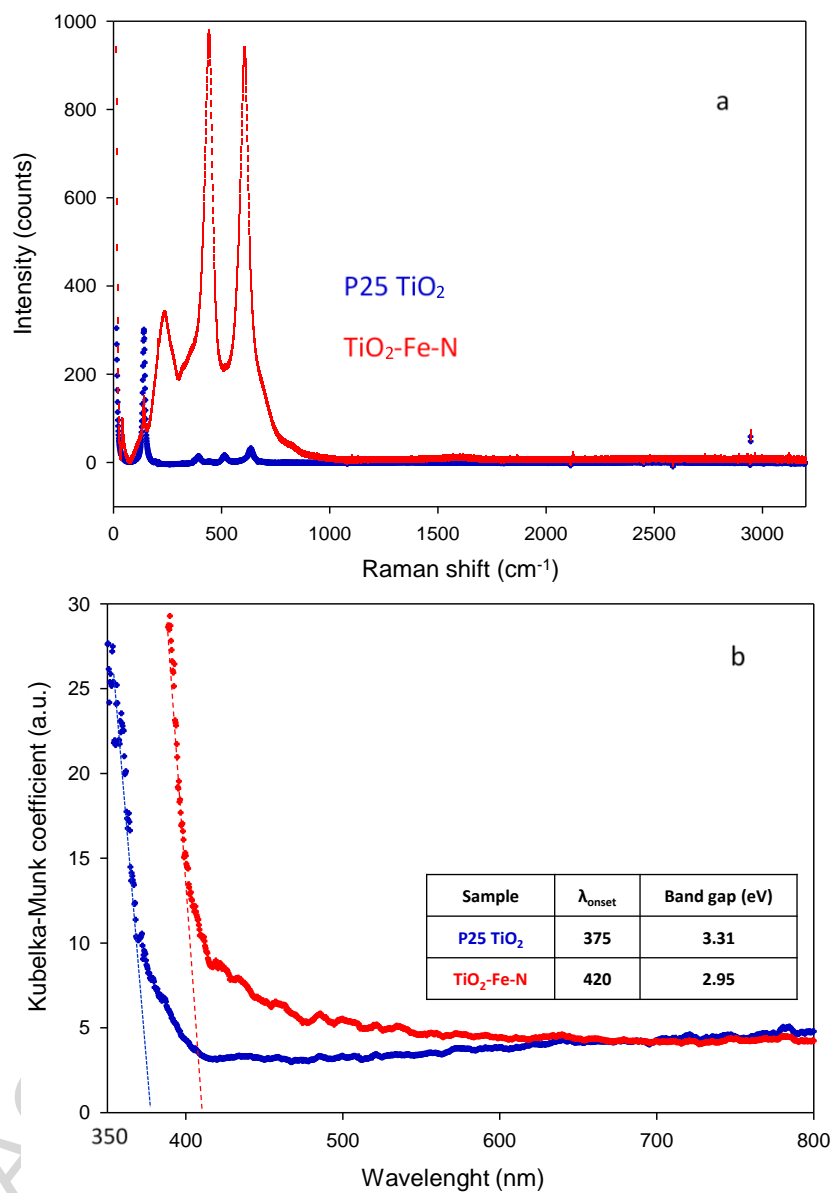


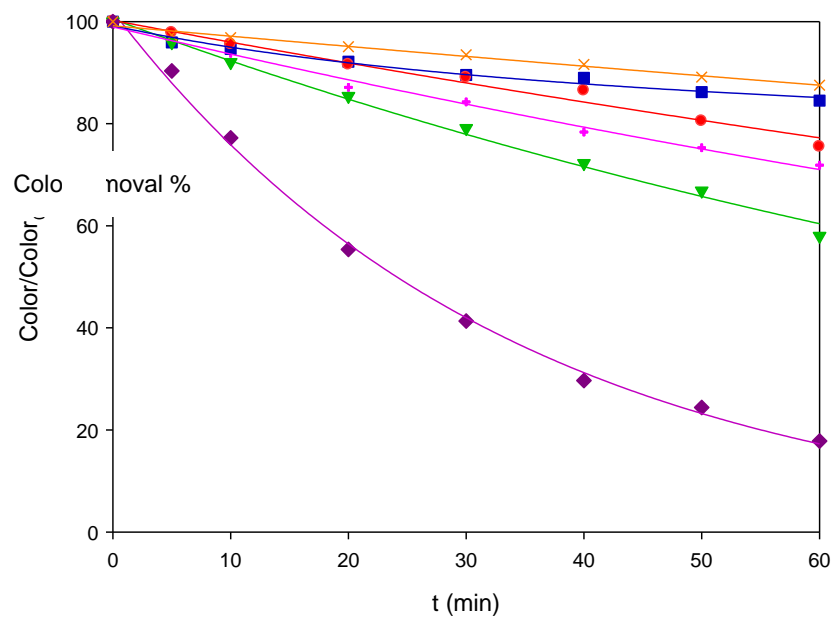
Figure 6.

Figure 7.

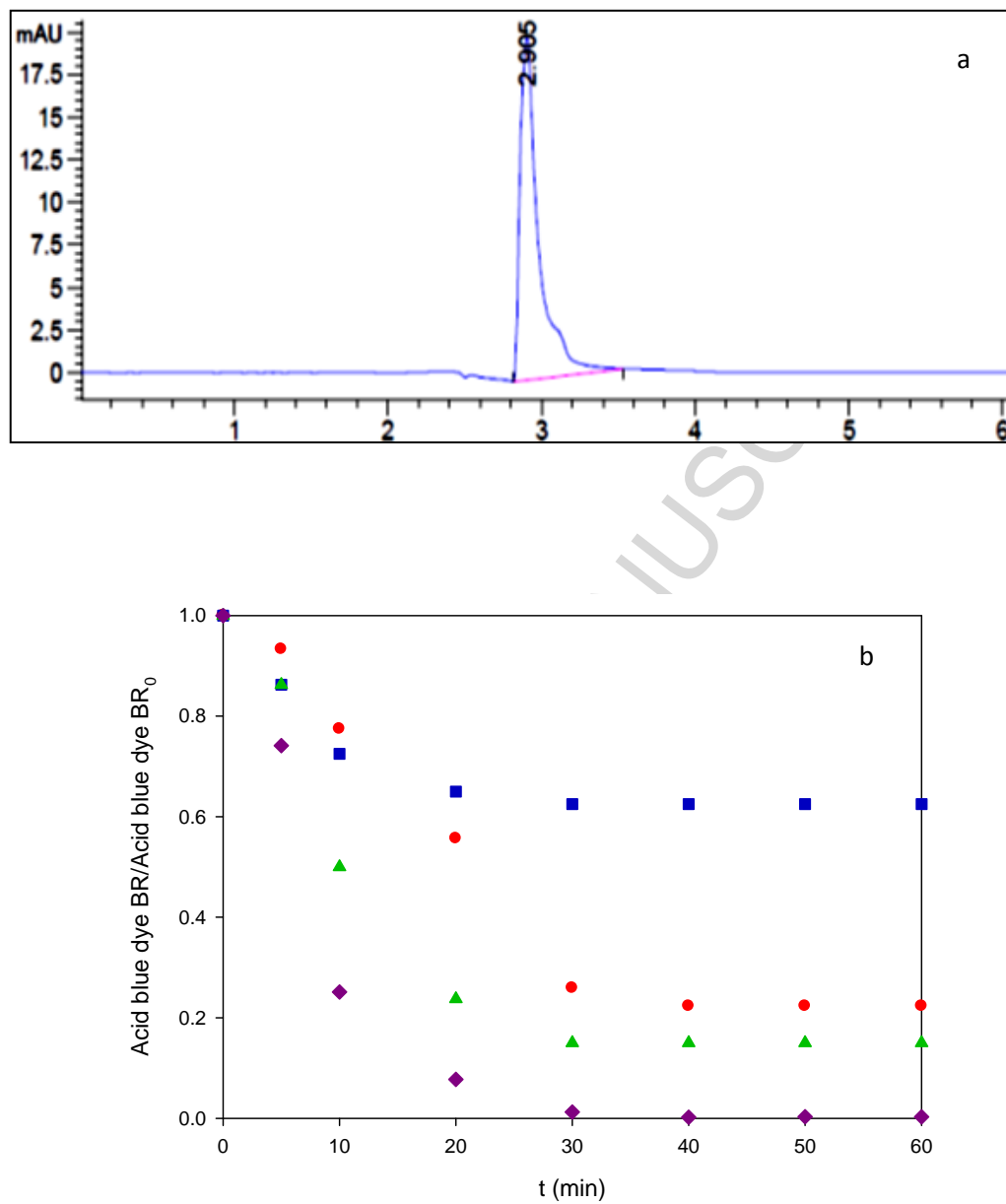


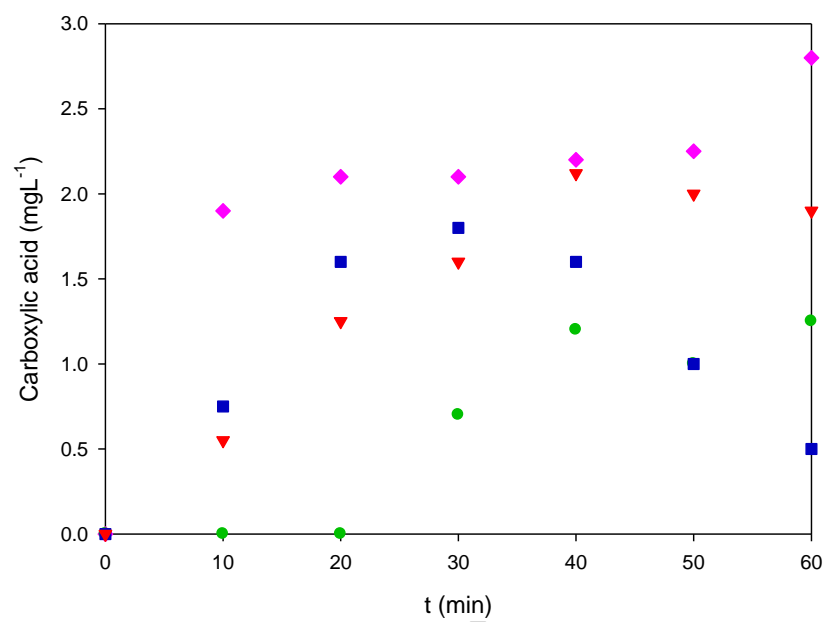
Figure 8.

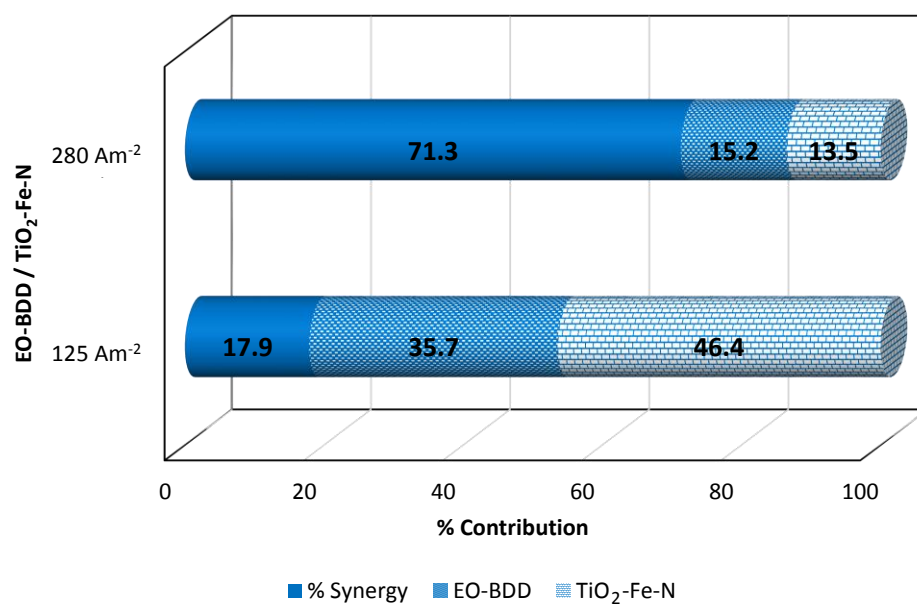
Figure 9.

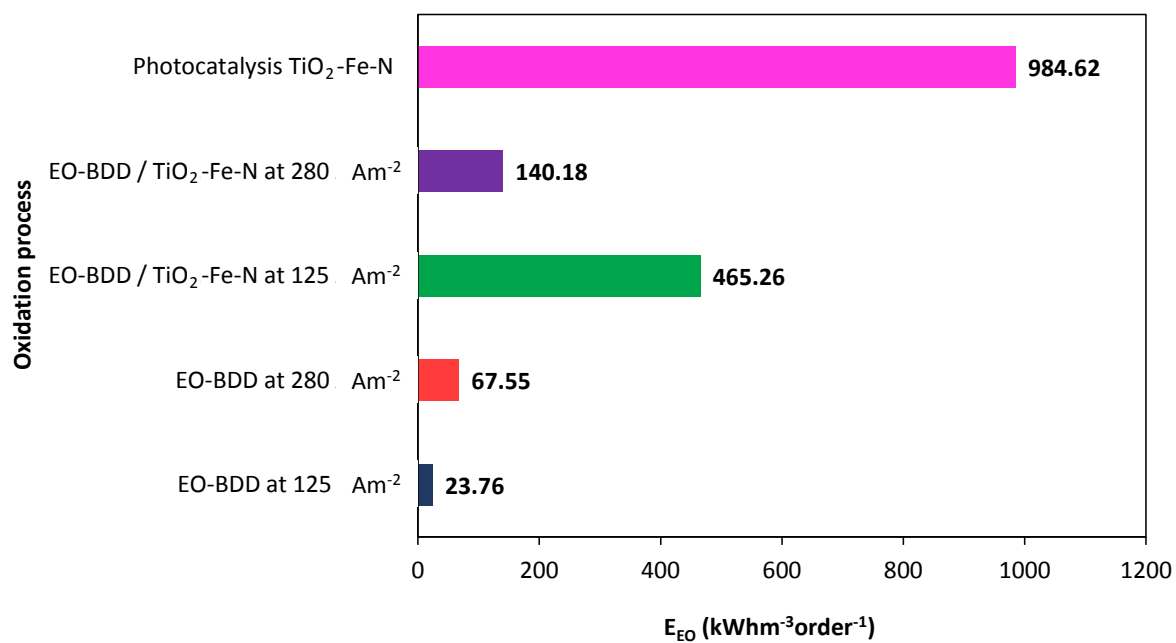
Figure 10.

Table 1

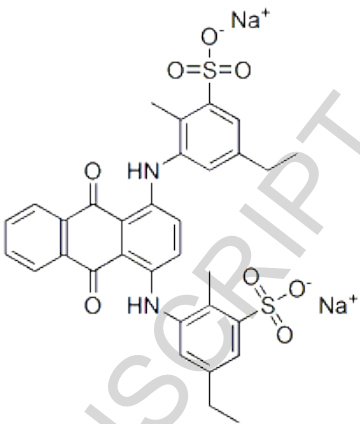
Acid blue BR	
Chemical formula	C₃₂H₂₈N₂Na₂O₈S₂
Chemical structure	
Molecular Weight:	678.68 g/mol

Table 2.

Oxidation processes	$k_{\text{color}} \text{ (min}^{-1}\text{)}$	R^2_{color}
EO-BDD at 125 Am ⁻²	3.00×10^{-3}	0.971
EO-BDD at 280 Am ⁻²	4.40×10^{-3}	0.985
EO-BDD / TiO ₂ -Fe-N at 125 Am ⁻²	8.40×10^{-3}	0.990
EO-BDD / TiO ₂ -Fe-N at 280 Am ⁻²	2.89×10^{-2}	0.997
Photocatalysis TiO ₂ -Fe-N	3.90×10^{-3}	0.989

Research Highlights

- Band gap value of $\text{TiO}_2\text{-Fe-N}$ is $2.95 < 3.31$ for TiO_2 Degussa P25
- $\text{TiO}_2\text{-Fe-N}$ material observed greater photoactivity than that of pure Degussa P25.
- 99% of acid blue dye BR degradation were achieved with acopled process.
- Coupling between electrochemical oxidation and photocatalysis observe major degradation.
- The process EO-BDD/ $\text{TiO}_2\text{-Fe-N}$ at 280 Am^{-2} allowed 78% of synergy,